Sussex Research Online

Interspersed distribution of selectivity to kinematic stimulus features in supragranular layers of mouse barrel cortex

Article (Published Version)

Martini, Francisco J, Molano-Mazón, Manuel and Maravall, Miguel (2017) Interspersed distribution of selectivity to kinematic stimulus features in supragranular layers of mouse barrel cortex. Cerebral Cortex, 27 (7). pp. 3782-2789. ISSN 1047-3211

This version is available from Sussex Research Online: http://sro.sussex.ac.uk/id/eprint/66101/

This document is made available in accordance with publisher policies and may differ from the published version or from the version of record. If you wish to cite this item you are advised to consult the publisher's version. Please see the URL above for details on accessing the published version.

Copyright and reuse:
Sussex Research Online is a digital repository of the research output of the University.

Copyright and all moral rights to the version of the paper presented here belong to the individual author(s) and/or other copyright owners. To the extent reasonable and practicable, the material made available in SRO has been checked for eligibility before being made available.

Copies of full text items generally can be reproduced, displayed or performed and given to third parties in any format or medium for personal research or study, educational, or not-for-profit purposes without prior permission or charge, provided that the authors, title and full bibliographic details are credited, a hyperlink and/or URL is given for the original metadata page and the content is not changed in any way.

http://sro.sussex.ac.uk

Cerebral Cortex, 2017; 1–8

doi: 10.1093/cercor/bhx019
Original Article

ORIGINAL ARTICLE

Interspersed Distribution of Selectivity to Kinematic Stimulus Features in Supragranular Layers of Mouse Barrel Cortex

Francisco J. Martini[1], Manuel Molano-Mazón[1,2] and Miguel Maravall[1,3]

[1]Instituto de Neurociencias de Alicante UMH-CSIC, Avda. Ramón y Cajal s/n, Campus de San Juan, 03550 Sant Joan d'Alacant, Spain, [2]Laboratory of Neural Computation, Center for Neuroscience and Cognitive Systems @UniTn, Istituto Italiano di Tecnologia, 38068 Rovereto, Italy and [3]Sussex Neuroscience, School of Life Sciences, University of Sussex, Brighton, UK

Address correspondence to Miguel Maravall, Email: m.maravall@sussex.ac.uk; Francisco J. Martini, Email: fmartini@umh.es

Abstract

Neurons in the primary sensory regions of neocortex have heterogeneous response properties. The spatial arrangement of neurons with particular response properties is a key aspect of population representations and can shed light on how local circuits are wired. Here, we investigated how neurons with sensitivity to different kinematic features of whisker stimuli are distributed across local circuits in supragranular layers of the barrel cortex. Using 2-photon calcium population imaging in anesthetized mice, we found that nearby neurons represent diverse kinematic features, providing a rich population representation at the local scale. Neurons interspersed in space therefore responded differently to a common stimulus kinematic feature. Conversely, neurons with similar feature selectivity were located no closer to each other than predicted by a random distribution null hypothesis. This finding relied on defining a null hypothesis that was specific for testing the spatial distribution of tuning across neurons. We also measured how neurons sensitive to specific features were distributed relative to barrel boundaries, and found no systematic organization. Our results are compatible with randomly distributed selectivity to kinematic features, with no systematic ordering superimposed upon the whisker map.

Key words: map, sensory coding, somatosensory, somatotopy, tactile, two photon, vibrissae, whiskers

Introduction

In the primary somatosensory "barrel" cortex, neurons responsive to the same whisker play different roles in representing the identity and location of objects contacted by the whisker (von Heimendahl et al. 2007; Jadhav et al. 2009; O'Connor et al. 2010; Petreanu et al. 2012; Safaai et al. 2013; Chen et al. 2013a; Clancy et al. 2015; Peron et al. 2015; Sofroniew et al. 2015). Barrel cortex neurons are tuned to diverse stimulus properties (Hires et al. 2012; Petreanu et al. 2012; Yamashita et al. 2013; Chen et al. 2013a; Sofroniew et al. 2015). Specifically, the dynamical or temporal stimulus features to which neurons are sensitive vary from cell to cell, providing a rich representation of stimulus dynamics at the population level (Estebanez et al. 2012). How are neurons with heterogeneous response properties distributed in space? Barrel cortex neurons with different selectivity to spatial stimulus characteristics (strength of tuning to principal whisker, tuning to direction of whisker deflection, or correlated motion of multiple whiskers) are found within each barrel column (Andermann and Moore 2006; Kerr et al. 2007; Sato et al. 2007; Kremer et al. 2011; Clancy et al. 2015; Estebanez et al. 2016).

© The Author 2017. Published by Oxford University Press.
This is an Open Access article distributed under the terms of the Creative Commons Attribution License (http://creativecommons.org/licenses/by/4.0/), which permits unrestricted reuse, distribution, and reproduction in any medium, provided the original work is properly cited.

A recent study of selectivity to different textures found that neurons preferring the same texture tend to cluster together across rat barrel cortex (Garion et al. 2014). Here, we examined the spatial distribution of neuronal selectivity to kinematic features of whisker motion using 2-photon calcium population imaging in mice, seeking to uncover systematic ordering principles.

Materials and Methods

Animal Preparation

All procedures complied with Society for Neuroscience, European, Spanish, and institutional policies for the care and use of animals in research. The protocol was approved by the local (Instituto de Neurociencias) bioethics and biosafety committee and by the institutional (CSIC) bioethics subcommittee. All experiments were performed under ketamine–xylazine anesthesia, and every effort was made to minimize suffering.

Female mice (CD1) at postnatal day ~30 were anesthetized using ketamine–xylazine (120 and 16 mg/kg body weight). The animal skull was exposed and cleaned and a metal plate attached with dental acrylic cement. A small craniotomy (~2 mm diameter) was made above barrel cortex. The location of the craniotomy was determined stereotactically (1.5 mm from Bregma, 3.4 mm from midline). Post hoc cytochrome-oxidase staining of tangential slices (see below) confirmed that the acquisition fields fell within the area corresponding to the caudal edge of the whisker pad. The exposed dura was covered with agarose. Eyelid and hindpaw reflexes were monitored throughout the experiments, and refresher ketamine–xylazine doses (20% of initial) added if necessary.

Stimulus Design

Although population calcium imaging permits analysis of tuning properties of neurons in terms of their spatial relationships, because of limitations in effective temporal resolution it is not ideal for an unbiased reverse correlation computation of receptive fields (Sharpee 2013). Our strategy was to construct a stimulus set that would capture features that neurons might selectively respond to (Jones et al. 2004; Arabzadeh et al. 2005; Petersen et al. 2008; Jadhav et al. 2009; Estebanez et al. 2012), while remaining small enough in size to permit adequate sampling during the course of an experiment. The set included idealized "position," "velocity," and "acceleration" filters, constructed by convolving the corresponding impulse functions with a Gaussian filter (Fig. 1B). Each waveform type was presented with 3 possible amplitudes, in the ratio 1:3:5. Stimuli were prepared in Matlab (Mathworks).

Whisker Stimulation

We inserted 10–15 contralateral vibrissae into a glass capillary tube glued to a piezoelectric bender (Physik Instrumente), placed 2–3 mm from the skin. This form of stimulation selected for neurons sensitive to correlated whisker motion, which are readily found in the barrel cortex and, in layer 2/3, are more numerous than those sensitive to uncorrelated motion (Estebanez et al. 2012, 2016). Since our aim was to examine whether different neurons have similar or diverse feature selectivity when interrogated with a common stimulus, motion of the piezoelectric actuator in the main set of experiments was always in the rostro-caudal direction.

Maximum deflection amplitude was 400 μm. Each deflection achieved a maximum speed of approximately 400 mm/s; speed only briefly remained close to maximum (median speed ~40 mm/s; for other parameters, see Pitas et al. 2016). These values are at the higher end of those used for passive stimulation in previous studies or recorded during free whisking in air (Kwegyir-Afful et al. 2008; Khatri et al. 2009), but in the range reached during natural whisker motion (Bagdasarian et al. 2013).

In a recording, each stimulus was presented 10 times; 4 recordings were done for each field of view, for a total of 40 repetitions per field. Consecutive deflections were separated by 1 s, an interval long enough to distinguish calcium transients (checked using electrophysiology; data not shown). Mechanical stimulation artifacts (resonances) were possible given the frequency range necessary to reproduce the deflection waveforms (~100 Hz). To rule them out, we used a custom-built optoelectronic device to check that the mechanical waveform described by the piezoelectric bender reliably followed the electrical input (Fig. 1B).

2-Photon Calcium Imaging

Calcium indicator in acetoxymethyl ester form (OGB1-AM, Life Technologies) was prepared by dissolving 50 μg of dye in 4 μL of 20% pluronic acid in DMSO (Life Technologies) and diluting (1:11) in artificial cerebrospinal fluid containing 100 μM Alexa Fluor 594 (for visualization; Life Technologies). Patch pipettes (tip diameter 2–4 μm) were pulled (Narishige), filled with dye solution and introduced into the cortex. The pipette tip was

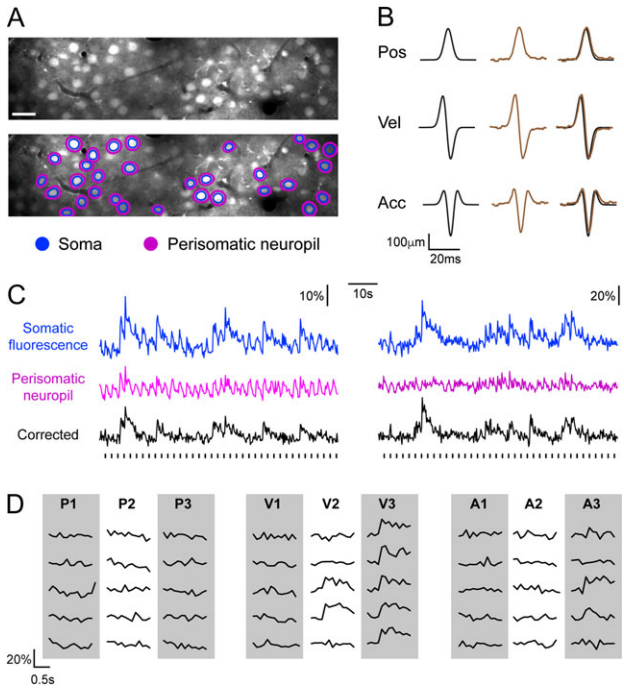

Figure 1. (A) Top, average projection of a movie showing cell bodies loaded with OGB. Bottom, same projection with regions of interest (blue) and neuropil halos (purple). Scale bar, 25 μm. (B) Waveforms of stimuli constructed as ideal position, velocity, and acceleration filters. Left, electrical input delivered to the piezoelectric actuator. Center, mechanical waveform recorded with an optical sensor. Right, superposition of input and mechanical output. (C) OGB fluorescence (blue) from 2 example neurons with corresponding perisomatic neuropil signal (halo, in purple) and corrected trace (black). Bottom trace, stimulus times. (D) Five examples of single-sweep calcium responses to different kinematic features in an example neuron. Each feature (P: position, V: velocity, A: acceleration) was presented in 3 different amplitudes (P1, P2, and P3 for position, for example). Different waveforms and amplitudes were in randomly interspersed order.

visualized under 2-photon scanning mode and gradually advanced to 100–150 μm below the cortical surface. Dye was pressure injected at 2–10 psi (Picospritzer) over 5–10 min. After injection, the pipette was withdrawn and the craniotomy covered with warm agarose (Sigma) and coverslipped. Imaging of whisker-evoked Ca^{2+} transients was performed using a 2-photon microscope (Leica TCS SP5 MP) with a Spectra Physics Mai Tai HP laser. Excitation wavelength was 830 nm. Cells were imaged using a 25× water-immersion objective (NA 0.95, Leica) at depths of 100–350 μm from the cortical surface. Full-frame images of 512 by 128 pixels were acquired at a spatial resolution of 1.48 pixel/μm; frame sampling rate was 8.8 Hz.

2-Photon Image Analysis

Images were registered with a modified StackReg ImageJ (NIH) plugin. For each movie, rigid transformation was performed using the first frame as reference. Experiments with excessive *x*-, *y*-, or *z*-axis fluctuations were discarded. Calcium responses were extracted using Caltracer 2.5, a Matlab (Mathworks) software package (Rafael Yuste Lab, Columbia University). Briefly, cells were visualized using the mean image of all frames and cell contours outlined automatically to define neuronal regions of interest (ROIs). Detected ROIs were supervised and adjusted manually if necessary. The mean raw fluorescence of each cell was estimated for all frames and background from unstained blood vessels subtracted (Greenberg et al. 2008). A perisomatic halo was drawn automatically in order to correct for neuropil contamination: halo fluorescence was scaled (optimal factor = 0.7) and subtracted from the background-subtracted mean fluorescence (Fig. 1A,C) (Kerlin et al. 2010; Chen et al. 2013b; Feinberg and Meister 2015). Finally, corrected fluorescence values were converted into $\Delta F/F_0$. Typically, responsive neurons had a skewed raw fluorescence distribution. F_0 was set to the eighth percentile of corrected fluorescence within a symmetric 6 s sliding window. Response amplitude was calculated as the difference between the mean $\Delta F/F_0$ value of the first 5 frames after a stimulus and the mean value of the last 3 frames before the stimulus.

Measurements of Response Properties

To assess whether to score neurons as tuned to kinematic features, we first computed the linear regression between magnitude of all calcium responses and amplitude of the corresponding stimulus waveforms for all neurons in a field of view. To correct for false discoveries of significantly tuned neurons in the simultaneously recorded population, we then applied the Benjamini–Hochberg–Yekutieli procedure for controlling the false discovery rate (corrected significance level: $P < 0.05$; fdr_bh Matlab function written by David Groppe) (Benjamini and Hochberg 1995; Benjamini and Yekutieli 2001). For neurons scored as tuned according to this procedure, and whose responses thus changed as a function of one or more stimulus parameters, we then defined tuning strengths for position, velocity, and acceleration as the respective coefficients of regression between response magnitude and stimulus waveform amplitude. Coefficients that did not reach the significance limit were set to zero. Where a neuron was significantly tuned to several features, we scored it as having mixed selectivity. Linear correlation and regression do not take into account the nonlinearities inherent to neuronal tuning and the conversion of a sensory stimulus into a change in calcium-dependent fluorescence (Peron et al. 2015). However, our approach provided a principled way to compare between the strength of responsiveness to different stimulus parameters defined over a similar time course. We also assessed tuning significance via direct shuffling of responses with respect to stimulus magnitude for each neuron (1000 repeats), with no qualitative change in results. Finally, we tested neurons for consistency of tuning properties across stimulus repetitions. Each ROI was recorded over 4 repeats of the stimulus set (see above), and the results given in the figures correspond to data collected over the entire set of 4 repeats. To check for consistency, data were split into 2 subsets consisting of the first and last pairs of recordings. 95% of neurons displayed identical tuning to at least one feature over the 2 subsets, and 81% displayed identical tuning to all 3 features, with no qualitative change in overall conclusions arising from splitting the data into subsets.

To measure the extent to which pairs of neurons in a field of view were similarly tuned we calculated the similarity index (SI). First, for each neuron in the field of view we constructed a tuning vector whose components were the cell's tuning strength (regression coefficient) for position, velocity, and acceleration (with tuning strengths not statistically significant entered as zero). Next, we computed the SI for each pair of neurons by taking the dot product of the 2 neurons' tuning vectors.

The slope of the linear fit between SI and the distance separating each pair of neurons was compared against that for shuffled values. Shuffled data were generated by randomly reassigning feature selectivity (regression coefficients) across neurons in the field of view, calculating the slope of the linear fit and then obtaining a mean slope for the field of view; shuffling was repeated 100 times. Pairwise correlations were calculated using the Spearman correlation coefficient computed for the entire corrected calcium fluorescence time series of the 2 cells, over the duration of the concatenated 4 recordings. We analyzed the dependence of neuronal correlations on distance by computing the slope of the linear fit between the 2 variables. Shuffled data for each experiment were constructed by randomly permuting the temporal order of responses to different stimulus presentations for each neuron in the field of view.

Histology and Barrel Field Reconstruction

In some experiments, brains were removed and fixed in 4% paraformaldehyde after imaging. The cortex was cut tangentially in 150 μm vibratome sections and stained for cytochrome oxidase. The barrel field was reconstructed and the acquired field localized in the reconstructed tissue. To place acquired fields in their original position, the pial vasculature of a fixed bright-field image was aligned using Photoshop (Adobe) with that from an in vivo bright-field picture of the same cortical surface. Then, using a single image of the cortical surface taken before starting the 2-photon acquisition, the fluorescent somata of layer 2/3 neurons in the field were aligned with the bright-field images. Distances to the closest barrel border were measured manually in Canvas (ACD Systems).

Results

To measure tuning to kinematic stimulus features, we imaged the activity of layer 2/3 neurons in ketamine–xylazine anesthetized mice ($n = 10$) while stimulating whiskers with controlled patterns (Fig. 1). To generate the stimulus set, we exploited the fact that neurons in the whisker pathway are tuned to kinematic stimulus features such as velocity or acceleration (Jones et al. 2004; Arabzadeh et al. 2005; Petersen et al. 2008; Jadhav

et al. 2009; Estebanez et al. 2012). We created a set of whisker deflection waveforms consisting of idealized "position," "velocity," and "acceleration" filters (Fig. 1B), each with 3 possible amplitudes. We reasoned that a neuron selectively sensitive to one of these features would exhibit responses whose size would covary preferentially with the amplitude of the corresponding waveform type. Different deflection waveforms and amplitudes were randomly interleaved in time. This stimulation produced clear calcium responses that allowed us to determine differential tuning of individual neurons to particular stimulus features (Fig. 1C,D).

In general, we considered that a neuron was tuned to a specific feature (position, velocity, acceleration) when the size of the calcium response displayed a significant relationship with the amplitude of the corresponding stimulus waveform (see Materials and Methods). Traces from an example neuron can be seen in Fig. 2A. For this neuron, calcium responses clearly grew with the amplitude of the velocity waveform, with increases in acceleration or position waveforms having a smaller effect (Fig. 2A,B). Reflecting this, the value of the regression coefficient between stimulus amplitude and neuronal response was greatest for velocity [r_p = 0.0069 for position (5–95% CI 0.0032–0.011); r_v = 0.0169 for velocity (CI 0.0132–0.021); r_a = 0.0106 for acceleration (CI 0.0073–0.0151); Fig. 2B].

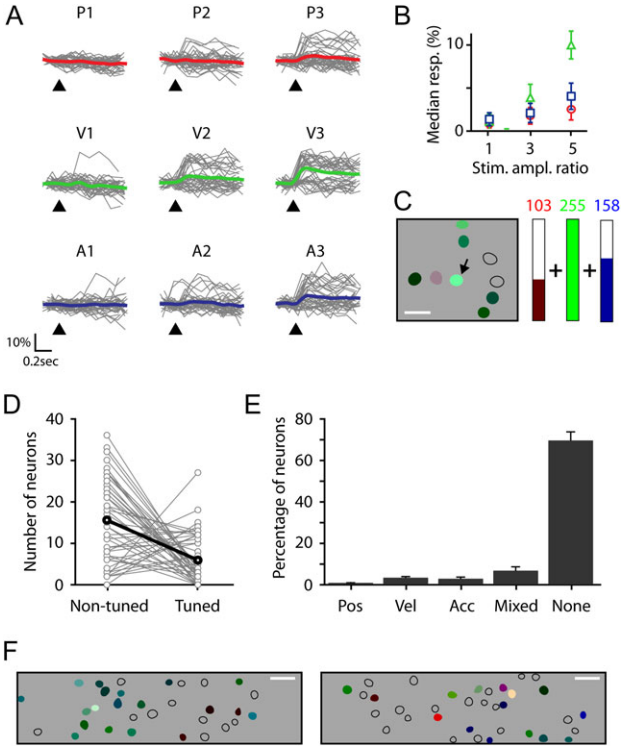

Figure 2. (*A*) All (gray) and average (colored thick trace) calcium responses to position (top), velocity (middle), and acceleration (bottom) stimuli in an example neuron. Arrowheads mark stimulus onset. (*B*) Plot of the median calcium responses and filter amplitudes for position (red circles), velocity (green triangles), and acceleration (blue squares) stimuli, for the same neuron. Stimulus amplitude is normalized to the smallest value. Tuning is strongest to velocity, as reflected in the steepest slope. (*C*) Mask of cell bodies used to quantify calcium changes from movies in an example field of view. Cell bodies are color-coded according to feature tuning (mixed selectivity allowed). The neuron in *A*–*B* is marked with a black arrow and its color depicted as a sum of red, green, and blue intensities proportional to the strength of its tuning to position, velocity, and acceleration, respectively. Outlined cell bodies do not respond or have no significant tuning. Scale bar, 25 μm. (*D*) Number of neurons with and without significant tuning to stimulus features in each field acquired. Thick black line, average. (*E*) Mean percentage of neurons with significant tuning to a single feature (Pos, Vel, Acc), mixed features or none. (*F*) Two further examples of the local distribution of kinematic feature selectivity within fields of view. Scale bars, 25 μm.

Where a neuron was significantly tuned to several features, we labeled it as having mixed selectivity (see Materials and Methods). Neurons throughout the whisker pathway, particularly in the barrel cortex, do not act as pure encoders of a single stimulus physical parameter or dimension; rather, their preferred features tile a space defined by multiple dimensions (Maravall et al. 2007; Petersen et al. 2008; Estebanez et al. 2012; Bale et al. 2013; Chagas et al. 2013; Maravall et al. 2013; Campagner et al. 2016). Thus, a characterization that allows for mixed selectivity better captures biological diversity. To display the tuning of each neuron visually, we used an RGB color map (Fig. 2C). We translated significant tuning strengths to color intensity levels by representing tuning to position as a red color intensity value, to velocity as green intensity, and to acceleration as blue intensity. The outcome for each neuron was a tone that mixed the appropriate intensities of red, green, and blue, reflecting tuning strength to position, velocity, and acceleration, respectively. Neurons with no significant tuning were depicted as outlines; neurons with significant tuning to a single feature were pure red, green, or blue (Fig. 2C,F; Supplementary Figs. 1 and 2 show identical data depicted in separate panels for the red, green, and blue channels). As the example neuron was tuned to velocity and (more weakly) to acceleration, it appears as bluish green in this representation (Fig. 2C, black arrow). Overall, 50.2% of neurons in the data set responded to whisker stimulation. The analysis evidenced both tuned and non-tuned neurons, with an overall majority of non-tuned cells (71.8% of all neurons were non-tuned; n = 10 mice, 49 fields of view, 1054 neurons; Fig. 2D,E). Within tuned neurons, all categories of selectivity were represented (Fig. 2E).

Neighboring neurons in primary sensory cortices share synaptic input (Harris and Mrsic-Flogel 2013). To assess whether this is reflected in similarities in the behavior of neurons at the population level, for each acquired field of view we computed pairwise correlations across all neuron pairs over the full duration of the recorded calcium time series (i.e. including whisker stimulation). An example raster plot capturing the activity of neurons in a field of view suggests that correlations across neurons in that region were higher than expected by chance (Fig. 3A). This is borne out by the distribution of correlation coefficients for that field of view (Fig. 3B); mean correlation coefficient was 0.14 ± 0.0062 compared with 0.0022 ± 0.0013 obtained by shuffling responses of different neurons across stimulus presentations (n = 31 neurons; see Materials and Methods). Taking all experiments into account, the correlation coefficient for the data set was 0.1004 ± 0.008 (mean ± SEM across fields of view), compared with 0.011 ± 0.0024 for shuffled data (n = 49 fields of view including n = 1054 neurons; $P = 1.11 \times 10^{-9}$; Wilcoxon signed-rank test; Fig. 3C). We also compared neuronal and neuropil response correlations by choosing ROIs within the neuropil in each field of view (10 ROIs per field) and repeating the analysis above. Neuropil responses were more correlated with each other than neuronal responses (for neuropil, mean ± SEM coefficient was 0.1792 ± 0.0097; n = 49 fields including n = 490 ROIs; vs. neurons, $P = 2.13 \times 10^{-7}$; Wilcoxon signed-rank test).

Previous publications in barrel cortex have shown correlated spontaneous and evoked activity between neurons, falling-off over distances ~160–200 μm (Kerr et al. 2007; Sato et al. 2007;

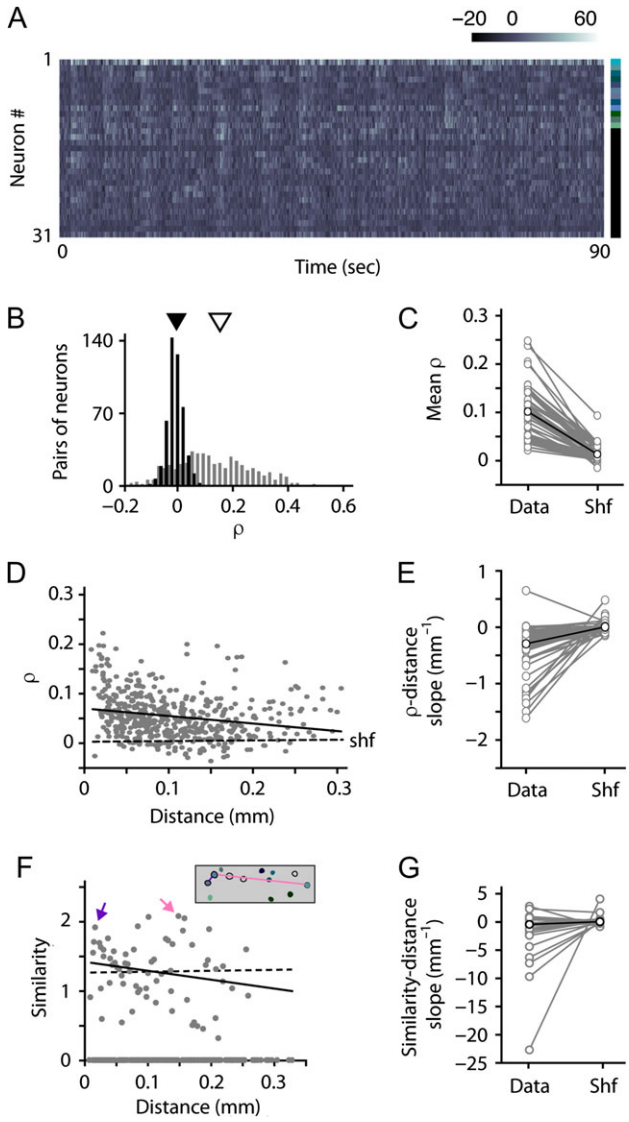

Figure 3. (*A*) Raster plot of calcium response activity for all neurons in an example field during a 90 s period of whisker stimulation. Feature tuning selectivity for each neuron is indicated in color code bar on right. (*B*) Distribution of correlation coefficients for pairs of neurons in the example field in *A* (gray). Shuffled data are shown in black. Average represented by arrowheads on top. (*C*) Mean correlation coefficient for each field acquired and for corresponding shuffled data; average in black. (*D*) Correlation coefficients as a function of distance between neurons for the example field in A. Linear fit for true (black solid line) and shuffled data (dashed line). (*E*) Slope of the linear fit between correlation coefficients and interneuronal distance for true and shuffled data for all fields; average in black. (*F*) Tuning SI as a function of distance between pairs of neurons for the field of view in A. Each dot corresponds to one pair of neurons. Arrows point to values for the color-coded connected pairs in the inset panel. Linear fit for true (black solid line) and shuffled data (dashed line). (*G*) Slope of the linear fits between SI and interneuronal distance for true and shuffled data for all fields; average in black.

Clancy et al. 2015). We examined the effect of distance on correlations over up to 300 μm. For the neurons in the raster plot of Fig. 3A, correlations decreased with distance, with a mean spatial gradient of −0.15 mm^{-1} (0.0025 mm^{-1} for shuffled data; Fig. 3D). Most of the fall-off in correlation occurred within the first 100 μm of distance between neurons. For the complete data set, the spatial gradient was −0.29 ± 0.062 mm^{-1} (median ± standard error of median [SEM]), significantly different than for shuffled data, −0.0062 ± 0.014 mm^{-1} (n = 49 fields of view; $P = 1.31 \times 10^{-8}$; Wilcoxon signed-rank test; Fig. 3E). Yet for experiments with pairs of neurons separated by over 200 μm, the spatial gradient decreased to −0.13 ± 0.17 mm^{-1}, compared with −0.109 ± 0.085 mm^{-1} for shuffled data (median, SEM; n = 30 fields of view with >4 pairs extending >200 μm; P = 0.106; Wilcoxon signed-rank test). Therefore, while nearby neurons showed correlated activity during stimulation, this correlation decreased with distance over a range ~200 μm, comparable to the diameter of a barrel column.

Because correlations in neuronal activity during stimulation were higher in nearby neurons, probably because of partially shared synaptic input, we wondered whether functional tuning would evidence spatial organization within comparable distances (~200 μm). To test this, we analyzed the similarity of response tuning as a function of distance between cells. We created an index (SI) to measure the extent to which the tuning of a pair of neurons was alike (Materials and Methods). We then plotted SI as a function of distance between the neurons in the pair (Fig. 3F). In some experiments, there appeared to be a relationship between SI and distance (for the example in Fig. 3F, spatial gradient = −1.29 mm^{-1}; compared with shuffled, 0.133 mm^{-1}; n = 29 neurons, n = 465 pairs). This was consistent with a visually apparent tendency for neurons to cluster in some of the fields of view (e.g. nearby green neurons in Fig. 2F, left panel). However, pooling across experiments indicated no consistent spatial organization of SI (median slope −0.467 ± 0.000675 mm^{-1}; for shuffled data, −0.0169 ± 0.119 mm^{-1}; n = 26 fields of view; P = 0.114; Wilcoxon signed-rank test; Fig. 3G). These results confirm a visual intuition from Fig. 2F: Functional responses to kinematic features are heterogeneous on a local scale, with neurons tuned to different features interspersed within the circuit.

Finally, we wondered if tuned neurons were systematically arranged relative to the barrel structure, for example, by asymmetric distribution between barrel- and septum-related territories. Thus, we examined the localization of tuned neurons relative to the histologically reconstructed barrel field map (n = 3 mice; respectively, n = 167, 102, and 117 imaged neurons, of which n = 59, 39, and 47 were tuned; imaged at depths ranging between 150–200, 190–220, and 135–185 μm, respectively; Fig. 4A,B; Supplementary Fig. 3 shows identical data in separate panels for the red, green, and blue channels). Tuned neurons were evenly distributed between barrel- and septum-related areas (38.8% and 35.8%, respectively were tuned; P = 0.58; Fisher exact test; Fig. 4C). We also tested whether neurons tuned to specific features were located preferentially relative to barrel or septum areas. To this end, we measured the horizontal distance of each significantly tuned neuron to the nearest barrel border. Neurons tuned to different features were not located differently relative to barrel borders, that is, relative to the columnar structure of barrel cortex (position vs. velocity: P = 0.77; position vs. acceleration: P = 0.70; velocity vs. acceleration: P = 0.68; Kolmogorov–Smirnov 2-sample test; Fig. 4D). Thus, we did not find evidence for spatial organization of kinematic feature tuning with respect to the barrel map in layer 2/3 of mouse barrel cortex.

Discussion

Neurons in the barrel cortex have strikingly heterogeneous response properties (Maravall and Diamond 2014). In layers 2/3 of the barrel field, neurons represent a wide range of spatial and temporal properties of whisker motion (Andermann and

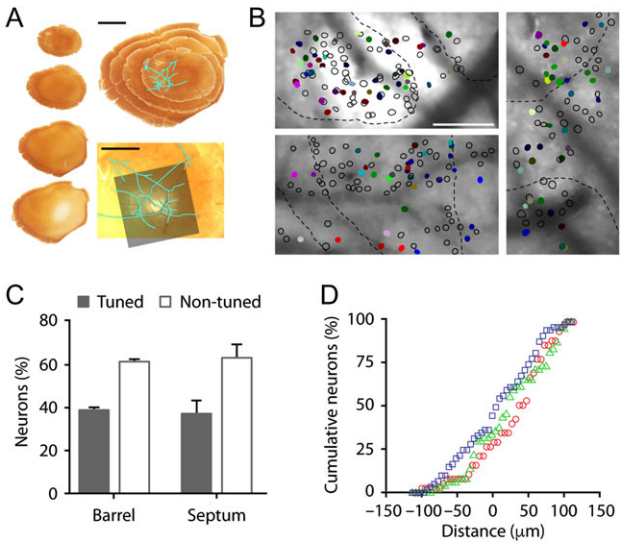

Figure 4. (*A*) Locating an imaged area in the barrel field map. Left column, cytochrome-oxidase staining in tangential slices to reconstruct the barrel field. Top right, drawing of superficial vascular plexus (cyan) from the fixed tissue reconstruction. Scale bar, 2 mm. Bottom right, alignment of the surface of the imaged area to the post hoc barrel field reconstruction by means of blood vessel registration. Scale bar, 1 mm. (*B*) Imaged neurons from 3 animals, color-coded according to feature selectivity, superimposed on the registered barrel reconstruction (black dashed line). Scale bar, 100 μm. (*C*) Percentage of tuned and non-tuned neurons over barrels and septa. (*D*) Cumulative distribution of distance to closest barrel border for neurons tuned to position (red circles), velocity (green triangles), and acceleration (blue squares). Barrel border is set to zero.

Moore 2006; Kerr et al. 2007; Sato et al. 2007; Jacob et al. 2008; Kremer et al. 2011; Estebanez et al. 2012; Garion et al. 2014; Peron et al. 2015; Estebanez et al. 2016). Here, we explored how neurons with sensitivity to different kinematic features are arranged. We found no ordering principle for feature selectivity—no systematically mapped representation. Instead, tuning follows an intermingled "salt-and-pepper" arrangement, with different neurons encoding for different features. This is reminiscent of the organization of orientation selectivity in rodent visual cortex (Ohki et al. 2005; Mrsic-Flogel et al. 2007). The overall correlation between responses of neuron pairs did fall-off with distance. This apparently counterintuitive difference between the ordered dependence of correlations on distance and the disordered distribution of feature selectivity is again similar to mouse visual cortex (Denman and Contreras 2014; Montijn et al. 2014). Diversity across differentially tuned subnetworks of neurons appears to be a common principle governing the local connectivity of primary sensory cortical areas in rodents (Bandyopadhyay et al. 2010; Rothschild et al. 2010).

We chose a simple stimulus set that exploits known feature selectivity in barrel cortex neurons, to provide adequate sampling of neuronal responses (Fig. 1*B*). These stimuli covered a limited region of the possible space to which neurons can be responsive (Jacob et al. 2008; Estebanez et al. 2012; Maravall and Diamond 2014). For example, neurons can be selectively driven by the amount of correlated motion across multiple whiskers; furthermore, layer 2/3 neurons are systematically arranged in relation to barrels and septa according to their sensitivity to correlated motion (Estebanez et al. 2016). Thus, a more extensive stimulation protocol could have identified feature selectivity in additional neurons. Our aim in using the present design was to bring out potential differences in selectivity across neighboring neurons, rather than to identify all possible stimulus features evoking responses.

In the study, around 50% of well-labeled supragranular neurons responded during our simple multi-whisker stimulation, and around 30% of neurons were selectively tuned to stimulus features. These figures are compatible with previous estimates in supragranular neurons of barrel cortex (with a relatively sparse fraction, ~20–30%, being highly tuned—regardless of stimulation paradigm) (Kerr et al. 2007; Sato et al. 2007; Jadhav et al. 2009; O'Connor et al. 2010; Yassin et al. 2010; Crochet et al. 2011; Barth and Poulet 2012; Estebanez et al. 2012; Margolis et al. 2012; Petersen and Crochet 2013; Chen et al. 2013a; Clancy et al. 2015; Peron et al. 2015; Sofroniew et al. 2015).

Our findings differ from a recent study that found spatial clustering of barrel cortex neurons tuned to the same texture (Garion et al. 2014). Several factors may have contributed to this difference. Important experimental differences include species (rat in the earlier study vs. mouse here), anesthesia (urethane vs. ketamine–xylazine) and form of stimulation ("electrical whisking" vs. passive). The former study also examined the build-up of responses during repeated stimulation, while we focused on tuning of responses temporally locked to a single, brief stimulus. In addition, two critical differences lie in the analysis. First, to build maps in the previous study, neurons preferring a particular texture, but potentially responding to others as well, were assigned that texture only. Instead, we chose to allow for mixed selectivity, since sensitivity to diverse, intermediate kinematic features is a hallmark of neurons in the whisker pathway (Petersen et al. 2008; Estebanez et al. 2012; Bale et al. 2013; Maravall et al. 2013). Second, the earlier study compared the true distribution of distances between neurons to a null hypothesis constructed by randomly and uniformly distributing an identical number of neurons across the entire field of view. This comparison did not provide a specific test for clustering of feature selectivity: A positive clustering result could arise simply from the imaged cell bodies being closer than expected had they been randomly scattered across the entire field of view. In contrast, our null hypothesis shuffled feature selectivity across neurons sited at their true locations, an approach designed to test for clustering specifically.

Supplementary Material

Supplementary material is available at *Cerebral Cortex* online

Funding

The Spanish Ministry of Science and Innovation (grant number BFU2011-23049, co-funded by the European Regional Development Fund); the Medical Research Council (grant number MR/P006639/1); the European Commission Horizon 2020 Programme, H2020-MSCA-IF-2015 (grant number 699829); the Valencia Regional Government (ACOMP2010/199).

Notes

We thank Jason Kerr for hosting M.M.-M. and providing advice, Stéphane Pages and Anthony Holtmaat for sharing analysis code, the Lagnado lab and Jamie Johnston for insightful discussion, and Giovanna Expósito for excellent technical help with the microscope set-up. All data supporting this study are available at http://crcns.org. *Conflict of Interest*: None declared.

References

Andermann ML, Moore CI. 2006. A somatotopic map of vibrissa motion direction within a barrel column. Nat Neurosci. 9: 543–551.

Arabzadeh E, Zorzin E, Diamond ME. 2005. Neuronal encoding of texture in the whisker sensory pathway. PLoS Biol. 3:e17.

Bagdasarian K, Szwed M, Knutsen PM, Deutsch D, Derdikman D, Pietr M, Simony E, Ahissar E. 2013. Pre-neuronal morphological processing of object location by individual whiskers. Nat Neurosci. 16:622–631.

Bale MR, Davies K, Freeman OJ, Ince RAA, Petersen RS. 2013. Low-dimensional sensory feature representation by trigeminal primary afferents. J Neurosci. 33:12003–12012.

Bandyopadhyay S, Shamma SA, Kanold PO. 2010. Dichotomy of functional organization in the mouse auditory cortex. Nat Neurosci. 13:361–368.

Barth AL, Poulet JF. 2012. Experimental evidence for sparse firing in the neocortex. Trends Neurosci. 35:345–355.

Benjamini Y, Hochberg Y. 1995. Controlling the false discovery rate - a practical and powerful approach to multiple testing. J R Stat Soc B Methodol. 57:289–300.

Benjamini Y, Yekutieli D. 2001. The control of the false discovery rate in multiple testing under dependency. Ann Stat. 29: 1165–1188.

Campagner D, Evans MH, Bale MR, Erskine A, Petersen RS. 2016. Prediction of primary somatosensory neuron activity during active tactile exploration. Elife. 5:e10696.

Chagas AM, Theis L, Sengupta B, Stuttgen MC, Bethge M, Schwarz C. 2013. Functional analysis of ultra high information rates conveyed by rat vibrissal primary afferents. Front Neural Circuits. 7:190.

Chen JL, Carta S, Soldado-Magraner J, Schneider BL, Helmchen F. 2013a. Behaviour-dependent recruitment of long-range projection neurons in somatosensory cortex. Nature. 499:336–340.

Chen TW, Wardill TJ, Sun Y, Pulver SR, Renninger SL, Baohan A, Schreiter ER, Kerr RA, Orger MB, Jayaraman V, et al. 2013b. Ultrasensitive fluorescent proteins for imaging neuronal activity. Nature. 499:295–300.

Clancy KB, Schnepel P, Rao AT, Feldman DE. 2015. Structure of a single whisker representation in layer 2 of mouse somatosensory cortex. J Neurosci. 35:3946–3958.

Crochet S, Poulet JF, Kremer Y, Petersen CC. 2011. Synaptic mechanisms underlying sparse coding of active touch. Neuron. 69:1160–1175.

Denman DJ, Contreras D. 2014. The structure of pairwise correlation in mouse primary visual cortex reveals functional organization in the absence of an orientation map. Cereb Cortex. 24:2707–2720.

Estebanez L, Bertherat J, Shulz DE, Bourdieu L, Leger JF. 2016. A radial map of multi-whisker correlation selectivity in the rat barrel cortex. Nat Commun. 7:13528.

Estebanez L, El Boustani S, Destexhe A, Shulz DE. 2012. Correlated input reveals coexisting coding schemes in a sensory cortex. Nat Neurosci. 15:1691–1699.

Feinberg EH, Meister M. 2015. Orientation columns in the mouse superior colliculus. Nature. 519:229–232.

Garion L, Dubin U, Rubin Y, Khateb M, Schiller Y, Azouz R, Schiller J. 2014. Texture coarseness responsive neurons and their mapping in layer 2-3 of the rat barrel cortex in vivo. Elife. 3:e03405.

Greenberg DS, Houweling AR, Kerr JN. 2008. Population imaging of ongoing neuronal activity in the visual cortex of awake rats. Nat Neurosci. 11:749–751.

Harris KD, Mrsic-Flogel TD. 2013. Cortical connectivity and sensory coding. Nature. 503:51–58.

Hires SA, O'Connor DH, Gutnisky DA, Svoboda K 2012. Encoding whisking-related variables in the mouse barrel cortex during object localization In. Society for Neuroscience Meeting. New Orleans.

Jacob V, Le Cam J, Ego-Stengel V, Shulz DE. 2008. Emergent properties of tactile scenes selectively activate barrel cortex neurons. Neuron. 60:1112–1125.

Jadhav SP, Wolfe J, Feldman DE. 2009. Sparse temporal coding of elementary tactile features during active whisker sensation. Nat Neurosci. 12:792–800.

Jones LM, Depireux DA, Simons DJ, Keller A. 2004. Robust temporal coding in the trigeminal system. Science. 304: 1986–1989.

Kerlin AM, Andermann ML, Berezovskii VK, Reid RC. 2010. Broadly tuned response properties of diverse inhibitory neuron subtypes in mouse visual cortex. Neuron. 67:858–871.

Kerr JN, de Kock CP, Greenberg DS, Bruno RM, Sakmann B, Helmchen F. 2007. Spatial organization of neuronal population responses in layer 2/3 of rat barrel cortex. J Neurosci. 27:13316–13328.

Khatri V, Bermejo R, Brumberg JC, Keller A, Zeigler HP. 2009. Whisking in air: encoding of kinematics by trigeminal ganglion neurons in awake rats. J Neurophysiol. 101:1836–1846.

Kremer Y, Leger JF, Goodman D, Brette R, Bourdieu L. 2011. Late emergence of the vibrissa direction selectivity map in the rat barrel cortex. J Neurosci. 31:10689–10700.

Kwegyir-Afful EE, Marella S, Simons DJ. 2008. Response properties of mouse trigeminal ganglion neurons. Somatosens Mot Res. 25:209–221.

Maravall M, Alenda A, Bale MR, Petersen RS. 2013. Transformation of adaptation and gain rescaling along the whisker sensory pathway. PLoS One. 8:e82418.

Maravall M, Diamond ME. 2014. Algorithms of whisker-mediated touch perception. Curr Opin Neurobiol. 25: 176–186.

Maravall M, Petersen RS, Fairhall AL, Arabzadeh E, Diamond ME. 2007. Shifts in coding properties and maintenance of information transmission during adaptation in barrel cortex. PLoS Biol. 5:e19.

Margolis DJ, Lutcke H, Schulz K, Haiss F, Weber B, Kugler S, Hasan MT, Helmchen F. 2012. Reorganization of cortical population activity imaged throughout long-term sensory deprivation. Nat Neurosci. 15:1539–1546.

Montijn JS, Vinck M, Pennartz CM. 2014. Population coding in mouse visual cortex: response reliability and dissociability of stimulus tuning and noise correlation. Front Comput Neurosci. 8:58.

Mrsic-Flogel TD, Hofer SB, Ohki K, Reid RC, Bonhoeffer T, Hubener M. 2007. Homeostatic regulation of eye-specific responses in visual cortex during ocular dominance plasticity. Neuron. 54:961–972.

O'Connor DH, Peron SP, Huber D, Svoboda K. 2010. Neural activity in barrel cortex underlying vibrissa-based object localization in mice. Neuron. 67:1048–1061.

Ohki K, Chung S, Ch'ng YH, Kara P, Reid RC. 2005. Functional imaging with cellular resolution reveals precise micro-architecture in visual cortex. Nature. 433:597–603.

Peron SP, Freeman J, Iyer V, Guo C, Svoboda K. 2015. A cellular resolution map of barrel cortex activity during tactile behavior. Neuron. 86:783–799.

Petersen CC, Crochet S. 2013. Synaptic computation and sensory processing in neocortical layer 2/3. Neuron. 78:28–48.

Petersen RS, Brambilla M, Bale MR, Alenda A, Panzeri S, Montemurro MA, Maravall M. 2008. Diverse and temporally precise kinetic feature selectivity in the VPm thalamic nucleus. Neuron. 60:890–903.

Petreanu L, Gutnisky DA, Huber D, Xu NL, O'Connor DH, Tian L, Looger L, Svoboda K. 2012. Activity in motor-sensory projections reveals distributed coding in somatosensation. Nature. 489:299–303.

Pitas A, Albarracin AL, Molano-Mazon M, Maravall M. 2016. Variable temporal integration of stimulus patterns in the mouse barrel cortex. Cereb Cortex. in press: doi: 10.1093/cercor/bhw006.

Rothschild G, Nelken I, Mizrahi A. 2010. Functional organization and population dynamics in the mouse primary auditory cortex. Nat Neurosci. 13:353–360.

Safaai H, von Heimendahl M, Sorando JM, Diamond ME, Maravall M. 2013. Coordinated population activity underlying texture discrimination in rat barrel cortex. J Neurosci. 33:5843–5855.

Sato TR, Gray NW, Mainen ZF, Svoboda K. 2007. The functional microarchitecture of the mouse barrel cortex. PLoS Biol. 5:e189.

Sharpee TO. 2013. Computational identification of receptive fields. Annu Rev Neurosci. 36:103–120.

Sofroniew NJ, Vlasov YA, Andrew Hires S, Freeman J, Svoboda K. 2015. Neural coding in barrel cortex during whisker-guided locomotion. Elife. 4:e12559.

von Heimendahl M, Itskov PM, Arabzadeh E, Diamond ME. 2007. Neuronal activity in rat barrel cortex underlying texture discrimination. PLoS Biol. 5:e305.

Yamashita T, Pala A, Pedrido L, Kremer Y, Welker E, Petersen CC. 2013. Membrane potential dynamics of neocortical projection neurons driving target-specific signals. Neuron. 80:1477–1490.

Yassin L, Benedetti BL, Jouhanneau JS, Wen JA, Poulet JF, Barth AL. 2010. An embedded subnetwork of highly active neurons in the neocortex. Neuron. 68:1043–1050.